NANO MICRO small

Supporting Information

for *Small*, DOI: 10.1002/smll.201702479

Miniaturized, Battery-Free Optofluidic Systems with Potential for Wireless Pharmacology and Optogenetics

Kyung Nim Noh, Sung Il Park, Raza Qazi, Zhanan Zou, Aaron D. Mickle, Jose G. Grajales-Reyes, Kyung-In Jang, Robert W. GereauIV, Jianliang Xiao, John A. Rogers, and Jae-Woong Jeong**

Submitted to small

Supporting Information

Miniaturized, battery-free optofluidic systems with potential for wireless pharmacology and optogenetics

By Kyung Nim Noh†, Sung Il Park†, Raza Qazi†, Zhanan Zou, Aaron D. Mickle, Jose G. Grajales-Reyes, Kyung-In Jang, Robert W. Gereau IV, Jianliang Xiao, John A. Rogers and Jae-Woong Jeong**

Kyung Nim Noh
Department of Electrical and Computer Engineering,
University of Illinois at Urbana-Champaign,
Urbana, Illinois 61801 (USA)
Prof. Sung Il Park
Department of Electrical and Computer Engineering;
Center for Remote Health Science Technologies,
Texas A&M University,
College Station, Texas 77843 (USA)
Raza Qazi
Department of Electrical, Computer, and Energy Engineering,
University of Colorado Boulder,
Boulder, Colorado 80309 (USA)
Zhanan Zou, Prof. Jianliang Xiao
Department of Mechanical Engineering,
University of Colorado Boulder,
Boulder, Colorado 80309 (USA)
Aaron D. Mickle, Jose G. Grajales-Reyes
Department of Anesthesiology,
Washington University Pain Center,
Washington University School of Medicine,
St. Louis, Missouri 63130 (USA)
Prof. Kyung-In Jang
Department of Robotics Engineering,
Daegu Gyeongbuk Institute of Science and Technology (DGIST),
Daegu 42988 (Republic of Korea)
Prof. Robert W. Gereau IV
Department of Anesthesiology, Department of Neuroscience;
Washington University Pain Center,
Washington University School of Medicine,
St. Louis, Missouri 63130 (USA)
Prof. John A. Rogers
Department of Materials Science and Engineering, Biomedical Engineering, Neurological Surgery, Chemistry, Mechanical Engineering, Electrical and Computer Science;
Center for Bio-Integrated Electronics; and Simpson Querrey Institute for BioNanotechnology,
Northwestern University,
Evanston, Illinois 60208 (USA)
Prof. Jae-Woong Jeong
Department of Electrical, Computer, and Energy Engineering,
Materials Science and Engineering Program,
University of Colorado Boulder,

Boulder, Colorado 80309 (USA)

School of Electrical Engineering,
Korea Advanced Institute of Science and Technology (KAIST),
Daejeon 34141 (Republic of Korea)

†These authors contributed equally to this work.

*To whom correspondence should be addressed. E-mail: jrogers@northwestern.edu (J.A.R.);

jeong.jaewoong@gmail.com (J.-W.J)

Keywords: optofluidic; fully implantable; battery-free; wireless; neural

Suppression of cross-coupling in the two-channel device (Figure 2)

To ensure independent operation of each channel, cross channel coupled power is assessed. At the frequency of the first channel (1.8 GHz), the S_{11} (reflected power) of the second channel is ~0.1 dB, which corresponds to ~2.2% of the input power. This means that 2.2% of the power delivered at 1.8 GHz will still be delivered to the second channel. However, 2.2% of the minimum required power of ~125 mW for the heater for fluid delivery in 25 seconds [1] is ~2.75 mW, which is not enough to activate an array of four μ-ILEDs, thereby supporting independent operation of the fluid delivery. Conversely, the power required for activating an array of μ-ILEDs is much lower than the power required for activation of the fluidic delivery, and thus the cross-channel coupling is less of concern for the second channel. The resonant frequency spacing can be further increased if larger cross channel isolation is required.

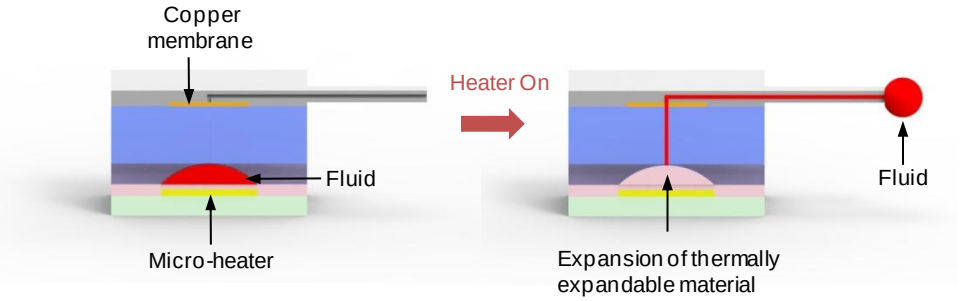

Figure S1. Operation principle of fluid delivery. Fluid is initially stored in the hemispherical reservoir (left). As the thermally expandable layer expands, fluid is pushed out throughout the microfluidic channel (right).

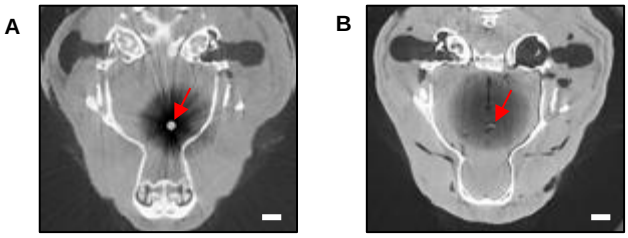

Figure S2. X-ray computed tomographic scans of the mouse brains implanted with a conventional metal cannula (A) and an optofluidic neural probe (B). The arrows indicate the implants. Compared to the metal cannula, the optofluidic probe causes physically less damage in the brain due to its smaller dimension. Scale bars, 1mm.

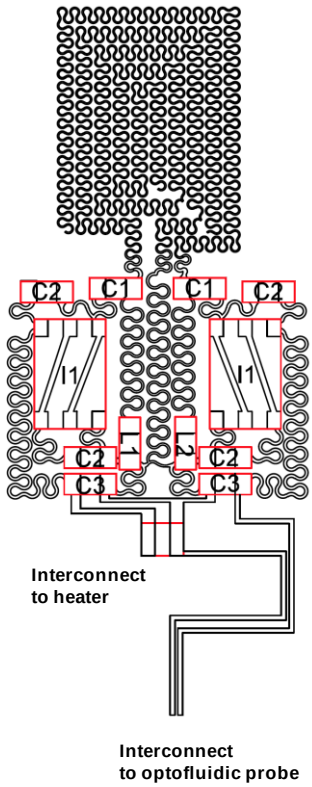

	Manufacturer	Part Number	Description
C1	Murata Electronics	GRM0335C1H1R0CA01D	1 pF Ceramic Capacitor
C2	Murata Electronics	GRM0335C1H220JA01D	22 pF Ceramic Capacitor
C3	Murata Electronics	GRM033R6YA104KE14D	0.1 µF Ceramic Capacitor
L1	Taiyo Yuden	HKQ0603U5N0C-T	5 nH Inductor
L2	Taiyo Yuden	HKQ0603U2N7B-T	2.7 nH Inductor
I1	Nexperia	1PS66SB82	Diode Array Schottky

Figure S3. Schematic layout and component information for RF energy harvester.

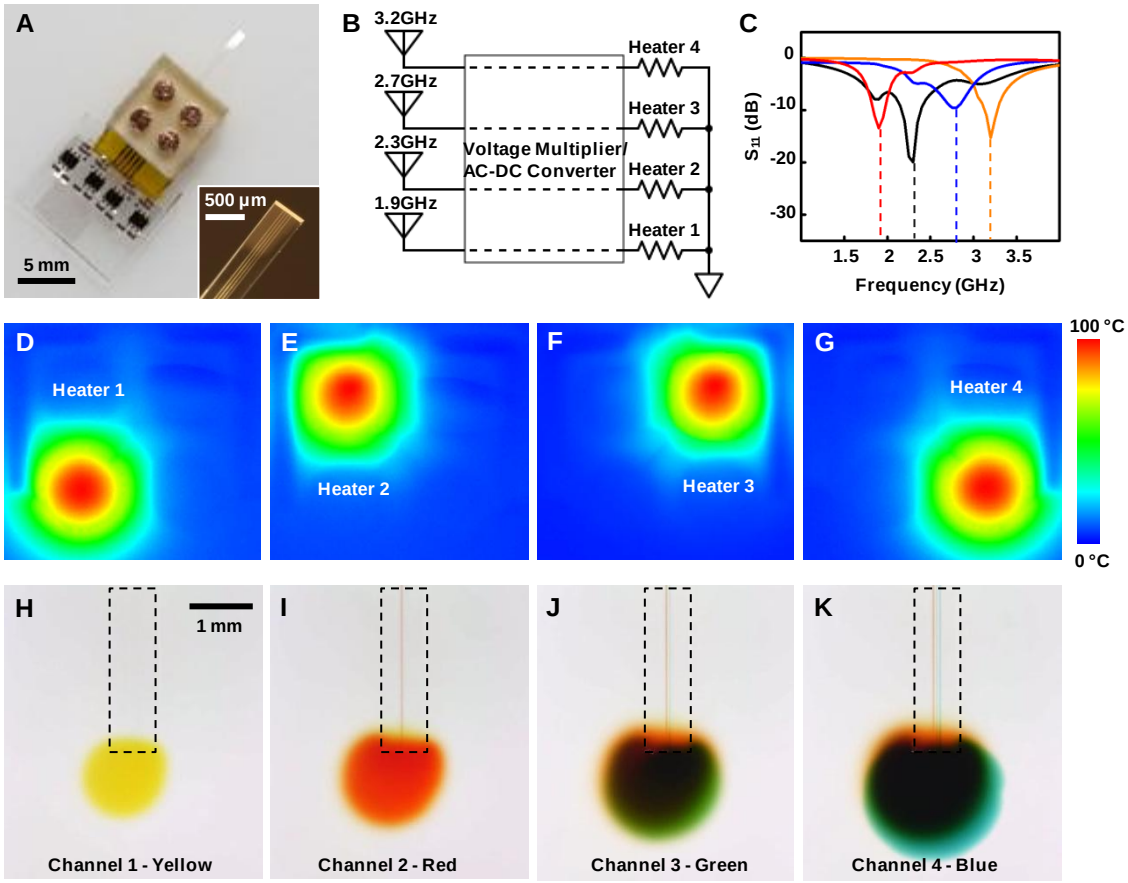

Figure S4. Fully wireless microfluidic device integrated with a stretchable four-channel RF energy harvester. A. Optical image of wireless microfluidic device, consisting of a stretchable four-channel antenna and four fluid reservoirs connected to the microfluidic probe. (Inset) Optical micrograph of a microfluidic probe with four separate channels. **B.** Block diagram illustrating selective channel operation of a four-channel wireless device. **C.** Scattering parameter, S_{11}, of the four-channel device. Channel 1–4 are operated at 1.9 GHz, 2.3 GHz, 2.7 GHz, and 3.2 GHz, respectively. **D–G.** IR images showing individual operation of four distinct heaters, each corresponding to a separate fluidic reservoir. **H–K.** Sequential images demonstrating capabilities of the wireless device for delivery of four distinct fluids (yellow, red, green, and blue dyes) throughout different individual microfluidic channels.

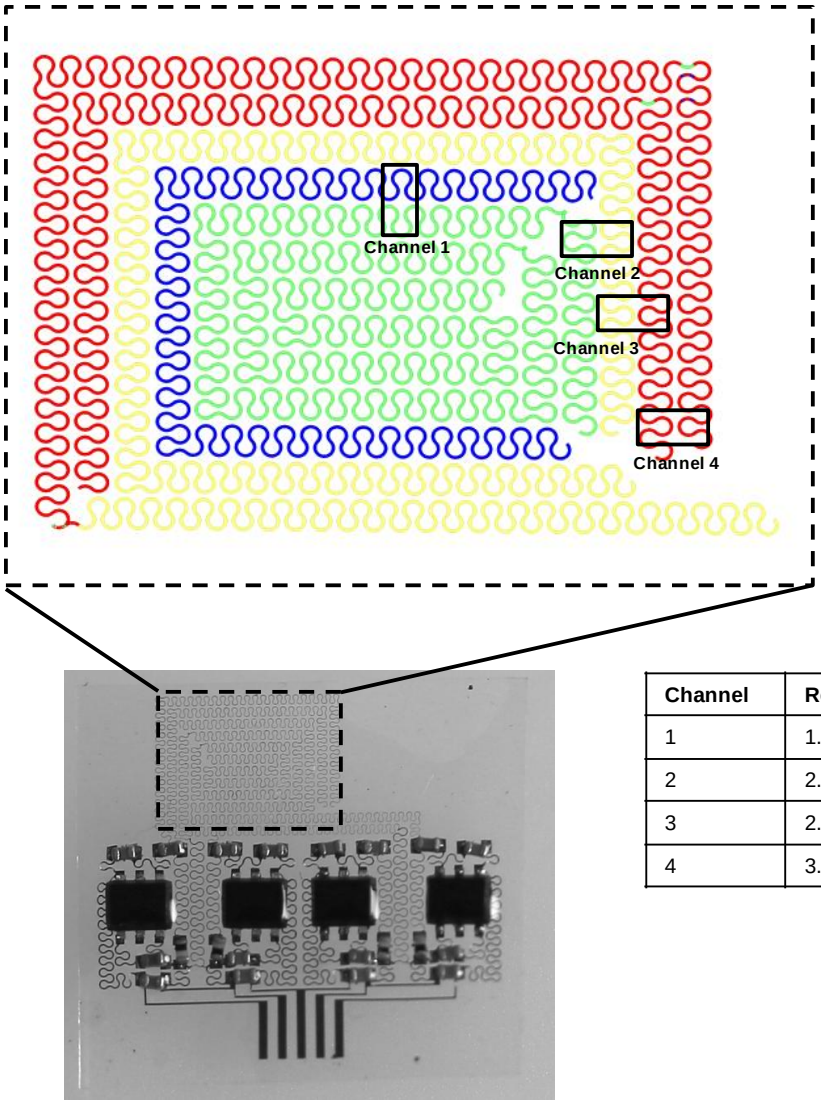

Channel	Resonant Frequency
1	1.9 GHz
2	2.3 GHz
3	2.7 GHz
4	3.2 GHz

Figure S5. Four-channel RF harvester antenna and resonance frequency at each channel. (Top) False-colored optical image of a stretchable RF antenna with four capacitive coupling channels. (Bottom) Optical image of the four channel RF harvester (left) and a table of channel numbers and its corresponding resonant frequencies (right).

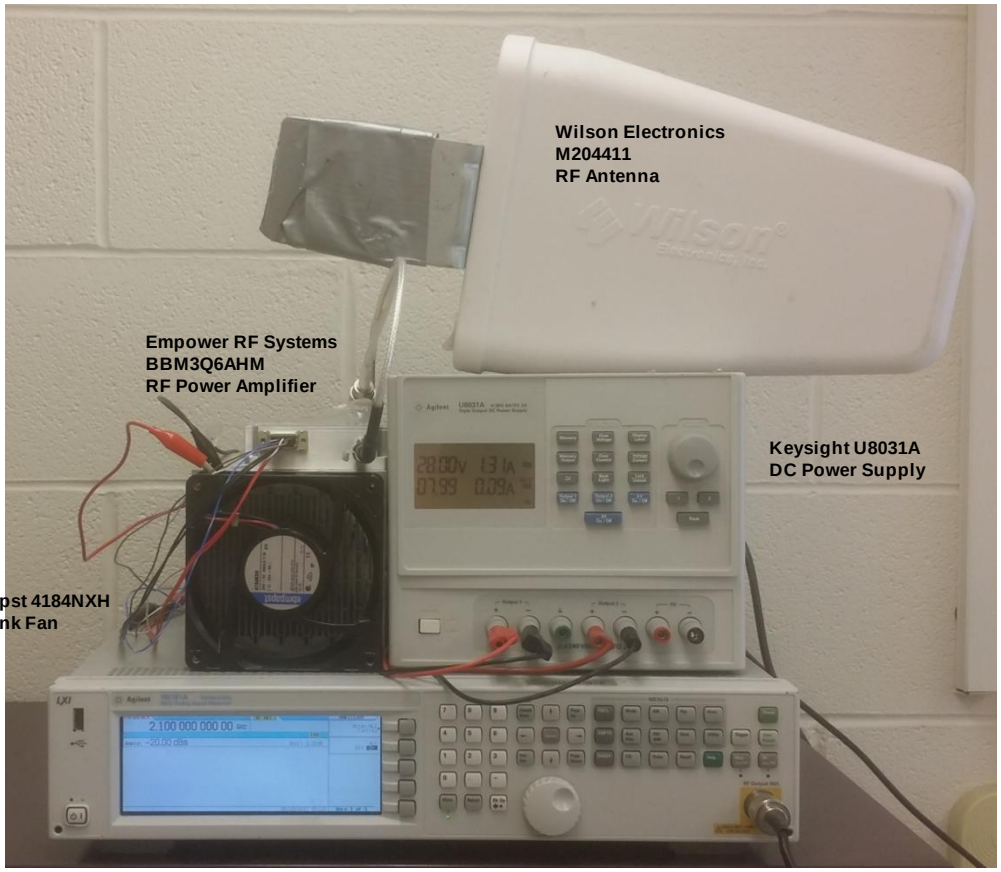

Figure S6. Picture of RF transmitter setup for control of wireless optofluidic devices.

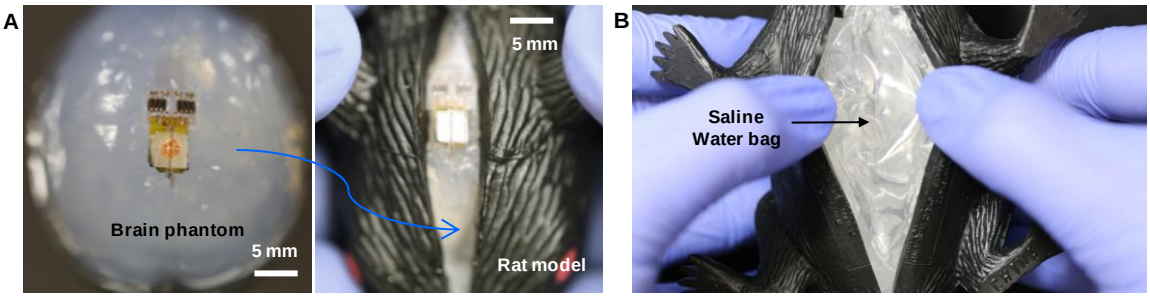

Figure S7. Preparation of a model rat for simulation of device operation. A. Images of an optofluidic device implanted into a phantom brain (0.6% agarose gel; left) and its integration in a model rat (right). **B.** Saline water bag inserted in the body of a model rat to simulate the RF characteristics of biological tissue.

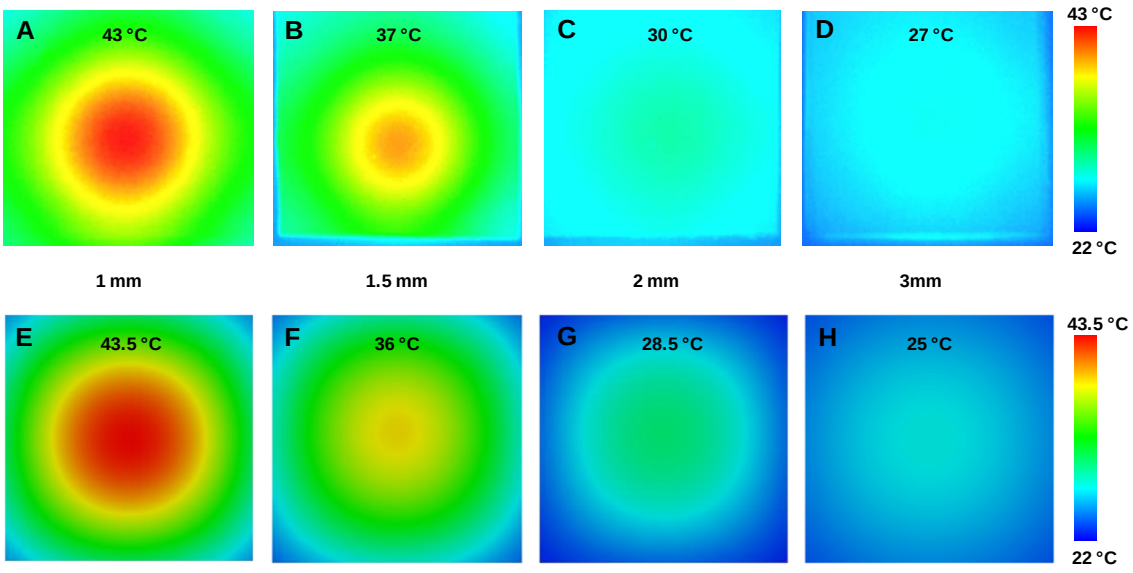

Figure S8. Temperature at the surface of PDMS layer encapsulating the thermally actuated pump for thermal insulation. IR images, **A–D**, show the temperature at device surface with a (**A**) 1 mm, (**B**) 1.5 mm, (**C**) 2 mm, and (**D**) 3 mm thick PDMS encapsulation layer. **E–H** show corresponding temperatures obtained by FEA simulation.

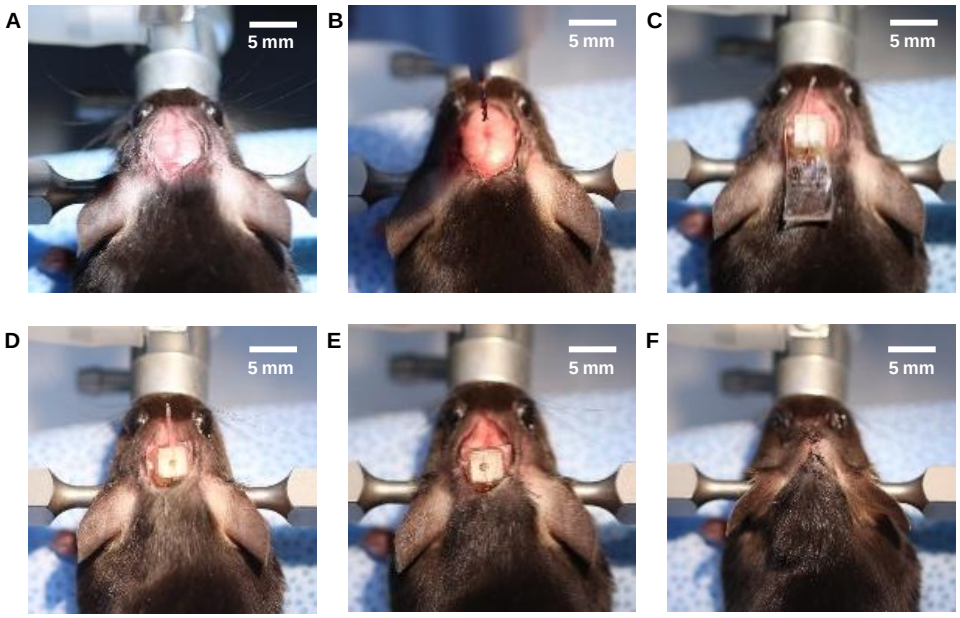

Figure S9. Proposed surgical procedure for implantation of optofluidic device in the mouse brain. A. The mouse's skull is exposed after a superficial midline incision is performed under aseptic conditions. **B.** Following the identification of the desired stereotaxic coordinates for the implantation of the device, we proceed to drill a small opening for placement of the optofluidic probe. **C.** Relative size of the implant with relation to the animal's head. **D.** Insertion of the soft RF harvester under the skin, caudal to the implantation site. **E.** Placement of the optofluidic probe into the brain cortex, following temporary stiffening of the implant with a biodegradable polymer (PLGA). **F.** After securing the implant, the mouse's skin was sutured to close the wound and allow for recovery.